Numerical simulation of wide band-gap AlGaN/InGaN light-emitting diodes for output power characteristics and emission spectra

Pankaj Shah[a] and Vladimir Mitin
Department of Electrical and Computer Engineering, Wayne State University, Detroit, Michigan 48202

Matt Grupen, G. Hugh Song, and Karl Hess
Beckman Institute, University of Illinois, Urbana, Illinois 61801

(Received 12 September 1995; accepted for publication 28 November 1995)

We present results from numerical simulations of AlGaN/InGaN double-heterostructure light-emitting diodes. A highly convergent, fast, and memory efficient algorithm necessary for wide band-gap device simulation was developed and is described here. Charge carrier tunneling currents and a band to impurity recombination mechanism are included. The results compare favorably to experimental results. The results demonstrate that the saturation of power at high currents, the high rate of increase in currents at high voltages, and the reduced broadening of the optical emission spectrum at high biases, with only band-to-acceptor recombination occurring in the active region, are due to carriers leaving the active region by thermionic emission rather than recombining. [S0021-8979(96)07505-7]

I. INTRODUCTION

There is a large effort underway to create optoelectronic devices from nitride-based compounds and alloys. The compounds AlN, GaN, and InN form a continuous alloy system whose direct band gap gives light emission from red to ultraviolet. Experimental groups throughout the world have created light-emitting diodes,[1] transistors,[2] and sensors[3] from these materials. Optically pumped nitride-based semiconductor lasers also have been created.[4] One of the main goals of this research effort is to create the world's first current injection pumped nitride-based semiconductor laser. Systems for imaging, information storage and retrieval and flat panel displays would benefit greatly from the blue light and smaller focal spot size available from these lasers. However, many difficulties are encountered in obtaining high quality materials required for the laser.

To create good devices the materials should be perfect and the structure optimized. Research on the growth of nitride based compounds and alloys is currently at a very early stage, and thus the material quality is not the best. However, the overall performance of the devices created is acceptable if one optimizes the structure and dopant concentration profile through numerical simulation. Simple modeling is not enough to fully understand and optimize the device. A complete self consistent numerical simulation should be performed, solving Poisson's equation, and the electron and hole continuity equations, to obtain information about current spreading, leakage current, tunneling of charge carriers, electric field distribution, and the recombination rates at different locations in the device. This will speed up the development of high quality devices based on these materials. People have already performed this kind of simulation for optoelectronic devices based on gallium arsenide[5] and other medium and narrow band-gap materials; however, the numerical simulations of wide band material devices performed up to now, to the best of our knowledge, are for very simple device structures based on material systems which do not include nitrides.

Numerical simulation of wide band-gap materials is more difficult than narrow band-gap materials because more mesh points are needed to resolve potential variations and charge concentrations due to the large range these values have. However, by using too many mesh points there is the risk of introducing large round off errors as well as the technical problems of requiring more computer memory and longer running times to solve the large system of coupled equations.

As a preparation for the simulation of nitride based lasers, we have simulated nitride-based light-emitting diodes (LEDs). In this paper we first discuss a new highly convergent, fast, and efficient algorithm for wide band-gap device simulation as well as methods for inclusion of charge carrier tunneling currents and band to impurity recombination of charge carriers. Then we will present results of a complete one-dimensional numerical simulation of a double-heterostructure AlGaN/InGaN/AlGaN LED.[1,6] Two cases were considered in our simulation: first, devices with band-to-acceptor recombination in the active region of the LED, and second, devices with band-to-band recombination in the active region. Different experimental works have seen emission from only impurity levels,[7] from both band-to-band and band-to-impurity level with relatively equal strengths[8] or where band-to-band and band-to-impurity recombination take place with emission strongest from band-to-impurity recombination.[9] The dominant recombination mechanism apparently depends on many things including what type of buffer layer is used, and what dopant atoms are involved.

The results give some insight into the processes taking place in this device. The results presented show that it is possible to optimize the output power and spectral content of light emission by proper doping and band-structure engineering.

[a]Electronic mail: shah@ciao.eng.wayne.edu

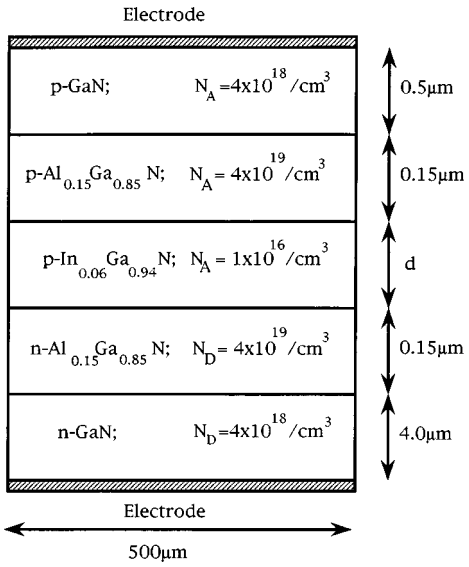

FIG. 1. Structure of the simulated device with dopant concentrations and alloy composition fractions.

II. DEVICE STRUCTURE

The light-emitting diodes simulated in this paper consist of a *p-i-n* structure shown in Fig. 1. This contains large charge carrier stopper layers adjacent to the active region in both the conduction and valence bands to confine carriers to the active region. A structure similar to this was fabricated and characterized by Nakamura and co-workers.[1] The InGaN center region is the active region where most of the light is emitted. The size of each region is shown in the figure. d is the active region's thickness. The compositions of the alloy layers, also shown in the figure, are the same as in Nakamura's experimental work.[1] The dopant concentrations were not available, so we assumed the values listed in the figure. Similar values are found in other experimental works with similar materials. Nakamura's device's active region was doped with Zn, from which the emission energy is 0.5 eV below the band-edge emission. We set the device's width to 500 μm and the length to 600 μm, which are similar to structures Nakamura fabricated previously.[10] These sizes were only used to convert current densities calculated by the program to currents for comparison with the experimental results of Nakamura.

III. MATERIAL PARAMETERS

Material parameters values for AlN, InN, and GaN, are listed in Table I. In the table, m_e^* and m_h^* are the effective masses of electrons and holes, respectively, relative to their free-space mass, μ_n and μ_p are the mobilities of electrons and holes, respectively, and $\epsilon_r(0)$ is the relative permittivity of the material at zero frequency. Parameter values for the alloy regions are obtained from

$$\text{value}(A_xB_{1-x}C) = \text{value}(AC)\times x + \text{value}(BC)\times(1-x). \tag{1}$$

Most of the values in the table were obtained from the best available experimental results published, though we have had to rely on theoretical values for a few of them. Different experiments and calculations have obtained different values for bowing parameters for AlGaN[11,12] and InGaN.[6] Also, the dependence of the electron affinities and thus the band discontinuities on alloy composition are not well known when bowing parameters are used to calculate the energy gaps. Therefore, we have decided not to use bowing parameters in the calculation of the energy gaps or electron affinities of the alloys. For the band offset between AlN and GaN, different experimental groups have made different measurements from $\Delta E_V = 0.8 \pm 0.3$ eV (Ref. 13) to $\Delta E_V = 0.5$ eV.[14] However, we are not aware of any experimentally obtained values for InN. Therefore, for consistency we have used the values listed in the table. The values listed in the table were obtained from an LCAO theory of heterojunctions[15] whose absolute values are not meaningful but relative values are. This procedure is more accurate for polar materials than ionic materials which nitride-based semiconductors are. This may explain why values in the table differ from experimentally obtained band offsets for AlN and GaN.

IV. SIMULATION PROCEDURE

Poisson's equation, and the electron and hole continuity equations were self consistently solved over a one dimensional cross section of the structure. This was done using an earlier version of the MINILASE[5] program which uses a modified Newton–Raphson method to solve the equations. For wide band-gap simulations, necessary modifications were made in the unknown variables and the solution algorithm. These were done to counteract two problems encountered. First, the range of variation in the unknown variables had to be reduced to improve convergence to a solution. The differ-

TABLE I. Material parameters of AlN, GaN, and InN.

Parameter	AlN	Ref.	GaN	Ref.	InN	Ref.	Units
m_e^*	$0.48m_0$	21	0.2	20	$0.12m_0$	26	⋯
m_h^*	$0.7m_0$	estimate	0.4	32	$0.5m_0$	26	⋯
μ_n	300	21	600	31	3000	37	$cm^2/V/s$
μ_p	14	25	9	22	300	estimate	$cm^2/V/s$
$\epsilon_r(0)$	8.5	30	9.0	30	15.0	30	⋯
Ref. index	2.15	30	2.67	30	3.0	30	⋯
Direct energy gap	6.2	38	3.43	29	1.9	30	eV
Electron affinity	7.64	28	10.23	28	11.1	28	eV
Spin orbit splitting	12	35	11	24	80	35	meV

ence between the majority and minority-carrier concentrations in a single region is many orders in magnitude (typically 20–40 orders of magnitude), and the minority-carrier concentration may fluctuate like noise during the simulation preventing convergence to a solution. Second, the built-in potential at equilibrium is quite large leading to large and sudden charge variations that need to be resolved. One possible way to counteract this problem of resolving charge variations is to use very fine meshes, but this would increase round off errors, increase the simulation time and require more computer memory.

To overcome these problems, first, the unknown variables were changed from $\mathscr{F}_0(\eta_n)$, $\mathscr{F}_0(\eta_p)$, and ψ to η_n, η_p, and ψ. Here $\mathscr{F}_0$ is the Fermi integral of order 0, and

$$\eta_n = \frac{E_{fn} - E_c}{kT}, \tag{2}$$

$$\eta_p = \frac{E_v - E_{fp}}{kT}, \tag{3}$$

where E_c and E_v are the coordinate-dependent conduction and valence band edges, and E_{fn} and E_{fp} are the electron and hole quasi-Fermi levels.

Then to obtain a converging solution for the on state of the light-emitting diode, a fast, iterative, and fully automated algorithm was developed and implemented where by the initial guess for one Newton iteration was obtained using the solution of a previous iteration that solved for a structure for which convergence was easier to obtain. First, we find the near equilibrium solution for a narrow gap device with a band structure whose form is similar to the device we eventually want to simulate. Then the device is turned on by slowly increasing the bias. Then the energy gap, electron affinity, and dopant concentrations are slowly increased in steps while occasionally increasing the bias to maintain the near on state of the device. This procedure continues until we obtain the actual wide band-gap device in its on state. The mesh's size does not have to be changed during the simulation. Therefore, this procedure allows one to use a mesh that is more coarse than one that is needed if the simulation started from equilibrium with the actual band structure, without reducing accuracy of the information obtained.

Tunneling currents at heterojunctions with large band discontinuities were also included. Tunneling currents should be included in wide band-gap device simulations, as we will demonstrate below, because the large band discontinuities at heterojunctions and high carrier concentration may create large narrow spikes in the conduction or valence bands causing tunnel currents to be a large fraction of the total current in the device. Finally, a band-to-impurity recombination mechanism was included.

A. Thermionic field emission

Highly accurate methods exist for the simulation of carrier transport through heterojunctions.[16] We use a very simple method for including tunneling into a general device simulation program with thermionic emission currents when a high degree of tunneling occurs at a heterojunction. In the present structure, the transmission coefficients for electrons at the base of the spikes in the conduction band are close to unity. Therefore, we assumed that all the carriers tunnel through the spikes.

This simplifies the usual procedure, based on the WKB approximation, for tunneling and thermionic emission at heterojunctions. Assuming all electrons tunnel through the band, to obtain the thermionic field emission current J_{TFE}, the electron's thermionic emission current at the junction is multiplied by a coefficient related to the height of the spike through which tunneling occurs Φ as

$$J_{\mathrm{TFE}} = J_{\mathrm{TH}} \times \exp(\Phi/kT), \tag{4}$$

where J_{TH} is the thermionic emission current for the case of no tunneling. During the simulations, the program automatically finds the height of the spike Φ for each applied bias by looking several nodes away from the junction on both sides of the junction. Tunneling and thermionic emission currents were incorporated only at mesh points on the edges of the heterojunctions and drift and diffusion currents were used at all other nodes in the device.

B. Recombination

Empirical parameters for recombination in these materials are not available. Therefore, we have calculated these rates. For band to band recombination, the recombination rates were calculated assuming the k-selection rule which states that the photon's momentum is zero throughout the recombination process. Thus we have the formula[17]

$$r_{\mathrm{sp},C-V}(E) = \frac{2\mu q^2 E |M_b|^2}{\pi m_0^2 \epsilon_0 h^2 c^3} \left(\frac{2m_r}{\hbar^2} \right)^{3/2} (E - E_g)^{1/2} \times f_c(E_c) f_v(E_v), \tag{5}$$

where $|M_b|$ is the average transition matrix element for the $k=0$ Bloch states, μ is the refractive index, q is the electron's charge, m_0 is the mass of a free electron, ϵ is the permittivity of free space, c is the speed of light, h is Planck's constant, and E_g is the energy gap. Using momentum and energy conservation, we have

$$E_c = \frac{m_r}{m_e}(E - E_g), \tag{6}$$

$$E_v = \frac{m_r}{m_h}(E - E_g), \tag{7}$$

$$m_r = \frac{m_e m_h}{m_e + m_h}, \tag{8}$$

where m_e and m_h are the electron and hole masses. The Fermi distribution functions for functions for electrons and holes are given by

$$f_c(E) = \frac{1}{\exp[(E/kT - \eta_n)] + 1}, \tag{9}$$

$$f_v(E) = \frac{1}{\exp[(E/kT - \eta_p)] + 1}. \tag{10}$$

The energy for holes is positive into the hole band.

For the average transition matrix element for the Bloch states the following formula is applicable:[18]

$$|M_b|^2=\frac{m_0^2E_g(E_g+\Delta)}{12m_e(E_g+\frac{2}{3}\Delta)}, \tag{11}$$

where Δ is the energy of the spinorbit splitting. This formula assumes a zinc-blende crystal structure and transitions between Bloch states obtained from Kane's model for the band structure. The nitride alloys and compounds occur naturally in the wurtzite structure; however, they are also grown in the zinc-blende structure. We assume both crystal structures behave similarly.

For recombination from the conduction band to the acceptor's energy level, the functional form of the acceptor's density of states was taken as a delta function and the conduction band was assumed parabolic. Summing the transition rate from Fermi's Golden rule over all states involved gives the recombination rate

$$r_{\mathrm{sp},C-I}(E)=\frac{4\pi\mu q^2E}{m_0^2\epsilon_0c^3h^2}f_c[E-(E_g-E_A)]f_v(-E_A) \times N_A\rho[E-(E_g-E_A)]|M_{if}|^2\times(V), \tag{12}$$

where E_A is the energy level of the acceptors above the valence band which in this case is 0.5 eV, ρ is the density of states in the conduction band, N_A is the density of acceptors, and V is the crystal volume. Here it is assumed that holes make the transition from the valence band to the acceptor level infinitely fast.

The k selection rule does not hold in band-to-acceptor recombination so an energy-dependent matrix element is used instead. We are interested in the performance of the device in its on state when the concentration of free carriers in the active region turns out to be much larger than the dopant concentration, and they strongly screen the dopants. Therefore the potential wells around the impurities are very narrow and the binding energy of the carriers to the impurities are decreased. Also the bohr radius of the impurity is roughly five times as large as the lattice constant. These allows us to say that the impurity behaves as a shallow impurity with a small ionization energy. Therefore we use a matrix element for a transition from a parabolic band to a shallow impurity. The energy level of the acceptors in Nakamura's material was experimentally measured[6] by photoluminescence (PL) experiments, during which the carrier concentration in the material may not be as high as when the LED is forward biased, and the screening and subsequent lowering of the ionization energy at the impurity did not occurred. Therefore the impurity level in the LED may actually have a smaller binding energy than the 0.5 eV measured by PL.

Thus the matrix element for this transition consists of the Bloch part given previously and an envelope part which includes factors for the influence of the impurity.

$$|M_{if}|^2=|M_b|^2|M_{\mathrm{env}}|^2, \tag{13}$$

where the envelope matrix element $|M_{\mathrm{env}}|^2$ is given by[18]

$$|M_{\mathrm{env}}|^2=64\pi a^{*3}(1+a^{*2}k_b^2)^{-4}V^{-1}, \tag{14}$$

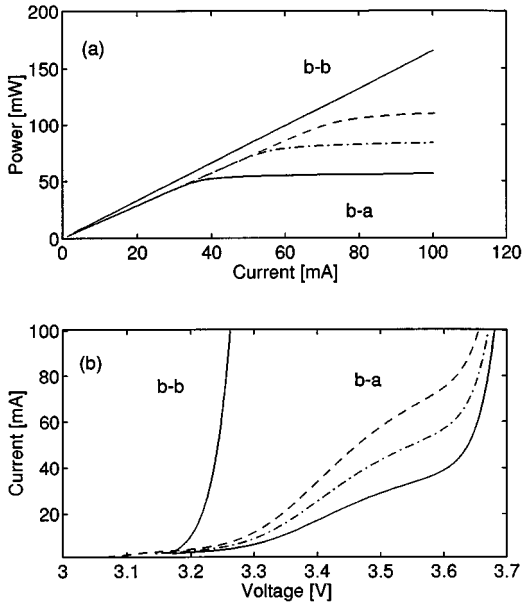

FIG. 2. Plots of (a) power vs current, and (b) current vs voltage for LEDs with active region thicknesses of 0.05 μm (—), 0.075 μm (–·–), and 0.1 μm (- -). (b-b) denotes band-to-band recombination and (b-a) denotes band-to-acceptor recombination in the active region.

where V is the crystal volume, a^* is the bohr radius and

$$k_b=\frac{\sqrt{2m_eE_e}}{\hbar}, \tag{15}$$

where E_e is the electron energy measured from the conduction band edge.

The total spontaneous emission rate for use in the continuity equations is given by

$$R_{\mathrm{sp}}(x,y,z)=\int_{-\infty}^{\infty}r_{\mathrm{sp}|\substack{C-I\\C-V}|}(E)dE. \tag{16}$$

V. RESULTS AND DISCUSSION

In this section we present results of the numerical simulations demonstrating the device performance when only band-to-band recombination occurs in the active region, and only band-to-acceptor recombination occurs in the action region. Effects of changing the active region's thickness, and dopant concentration on the power versus current plot, current versus voltage plot and optical emission spectra are discussed in the band-to-acceptor recombination case.

Figure 2(a) demonstrates the power versus current behavior for the device with only band-to-band recombination (b–b) and only band-to-acceptor (b-a) recombination. The curve for a 0.05-μm-thick active region is for comparison with the results of Nakamura. Also, shown are curves for active region thicknesses of 0.075 and 0.1 μm. This figure demonstrates that the power at a fixed current is higher for band-to-band recombination than band-to-acceptor recombination. For instance, with a 60 mA bias and an active region thickness of 0.05 μm and band-to-band recombination in the active region the optical power emitted is 99.0 mW, while if only band-to-acceptor recombination occurs, the optical

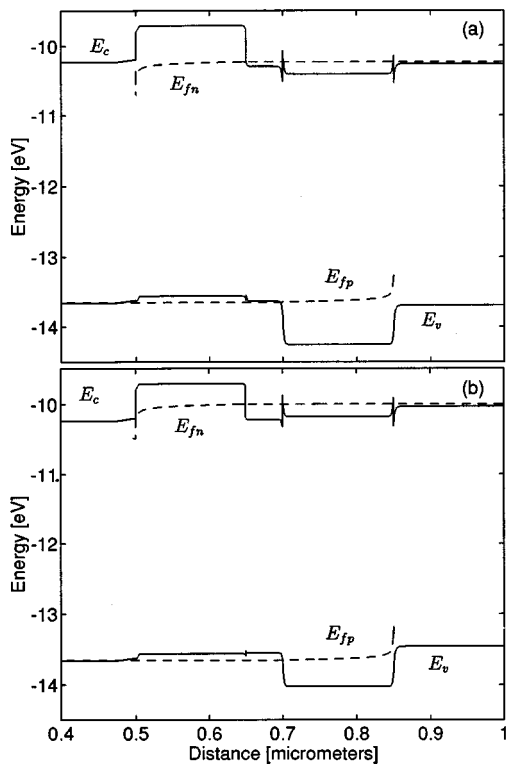

FIG. 3. Band structure of the 0.05-μm-thick active region device biased at (a) 20 mA and (b) 60 mA. E_c and E_v are the conduction and valence band edges, E_{fn} and E_{fp} are the electron and hole quasi-Fermi levels, respectively.

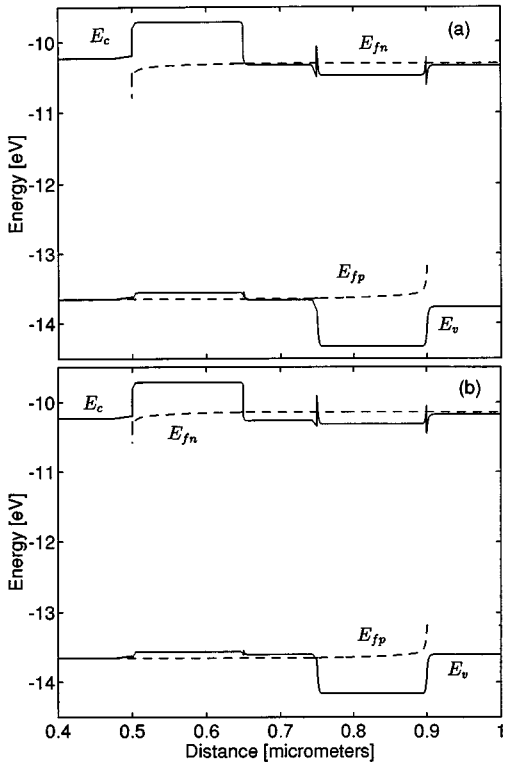

FIG. 4. Band structure of the 0.1-μm-thick active region device biased at (a) 20 mA and (b) 60 mA. E_c and E_v are the conduction and valence band edges, E_{fn} and E_{fp} are the electron and hole quasi-Fermi levels, respectively.

power emitted is 54.7 mW. This difference is due a higher recombination rate and also to the higher energy photons emitted. Also we observe that the power begins to saturate in the band to acceptor recombination plot as the current applied increases, and that this saturation occurs at higher currents when the active region is thicker. This saturation behavior is also observed in Nakamura's power vs current plots,[6] as well as in other groups' results[19] with different devices based on wide band-gap materials.

Figure 2(b) demonstrates the current versus voltage behavior for the same devices. Here we observe that to obtain the same amount of current, lower voltages are needed in the case of band-to-band recombination in the active region. Also, in the band-to-acceptor recombination case the rate of current increase is slow at low voltages and fast at high voltages.

The band structure plots in Fig. 3 explain the saturation in power and large increase in current when only band-to-acceptor recombination occurs in the active region. Figure 3(a) shows the band structure near the active region in the device with a 0.05-μm-thick active region biased at 20 mA and Fig. 3(b) shows the band structure near the active region when the device is biased at 60 mA. Quasi-Fermi levels for minority carriers in the outer layers are not shown because in this region their concentrations are negligibly small and all phenomena are determined essentially by the majority carriers. Electrons approach the active region from the right and holes from the left. Huge stopper layers are adjacent to the active region to confine the charge carriers to the active region. The conduction bands' edges also displays spikes through which charge carriers tunnel.

As the bias increases from Fig. 3(a) to Fig. 3(b) the active region's quasi-Fermi levels move further into the bands and the stopper layers are less effective at confining charge carries. Therefore, carriers leak out without recombining. The reason this occurs with band-to-acceptor recombination and not band-to-band recombination is that in the band-to-acceptor case a bottleneck exists due to the limited number of acceptors sites available for recombination.

Any method of increasing the rate of recombination in the device will reduce the loss of carriers out of the active region by mechanisms other than recombination. One method is to increase the thickness of the active region. This increases the number of recombination centers available in the active region and also the time during which carriers have a chance to recombine. The band structure for the same device with an active region thickness of 0.1 μm is shown in Fig. 4(a) with a bias of 20 mA and in Fig. 4(b) with a bias of 60 mA. Here the quasi-Fermi energy levels do not move as deep into the bands for the same bias as in the thin active region case shown in Fig. 3.

These band-structure diagrams also explain the rapid increase in currents at higher bias voltages. At low voltages the current is due mostly to recombination in the active region; however, at high voltage, the current is due to recombination in the active region and thermionic emission out of the active region.

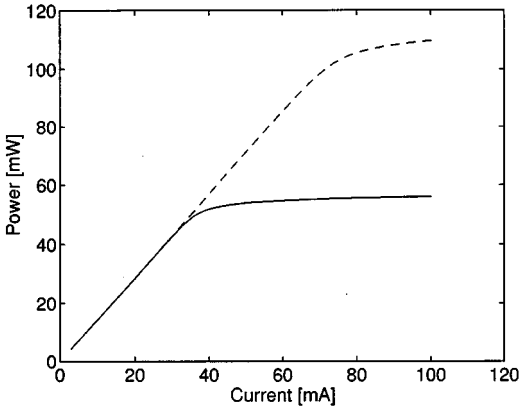

FIG. 5. Power vs current plot for an active region with an acceptor concentration of $2\times10^{16}/cm^3$ (- - -) and $1\times10^{16}/cm^3$ (—).

Increasing the concentration of the dopants in the active region also increases the chance of recombination and the power emitted when saturation occurs in the power versus current plot. Figure 5 demonstrates that when the concentration of the Zn acceptors in the active region doubles from 1×10^{16} to $2\times10^{16}/cm^3$ the output power also doubles. In this case the optical power emitted begins to saturate at a bias current of 65 mA rather than at 30 mA.

Figures 6(a) and 6(b) demonstrate the emission spectra for devices with only band-to-impurity recombination in the active region and a 0.05-μm-thick and a 0.1-μm-thick active region, respectively. Figure 6(c) demonstrates the emission spectra for a device with a 0.05-μm-thick active region with only band-to-band recombination. All plots are for bias currents of 20, 40, and 60 mA going from narrowest to widest. Figure 6(a) shows that for band-to-acceptor recombination, along with saturation of the output power, the increase in the height and width of the optical emission spectrum is much less for higher currents. This occurs because electron leakage out of the active region by thermionic emission is greater at high bias limiting the movement of the quasi-Fermi levels further into the band and the width of the emission spectrum is determined by the separation of the electron and hole quasi-Fermi levels. This behavior has been experimentally observed.[23] Figures 6(a) and 6(b) also show that thinner active region devices have a wider emission spectra for the same amount of bias current. This is because in the thin active region device the quasi-Fermi levels are deeper in the energy bands and further away from the energy gap for a given amount of bias current as demonstrated in Figs. 3 and 4 and thus the carriers which recombine are spread over a larger energy range. The uniformly growing optical emission spectra of band-to-band recombination is demonstrated in Fig. 6(c). Also, these spectra are much narrower than in Figs. 6(a) and 6(b) because the recombination bottleneck is not present and thus the quasi-Fermi levels do not move as far into the energy band for a given amount of bias current. Finally, we see that band-to-band recombination has a higher rate than band-to-acceptor recombination at high currents and a lower rate at low currents.

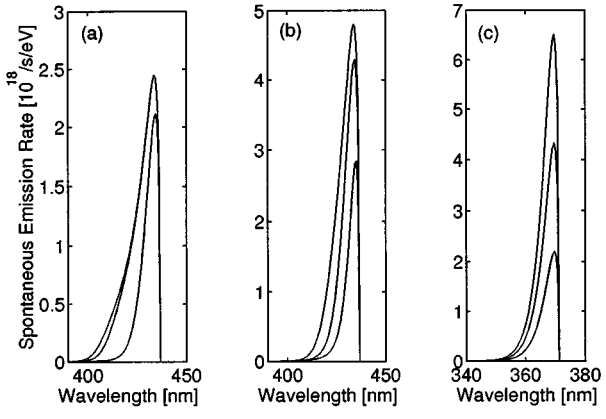

FIG. 6. Light emission spectra for a (a) 0.5-μm-thick active region with only band-to-acceptor recombination, (b) 0.1-μm-thick active region with only band-to-acceptor recombination, and (c) 0.05-μm-thick active region with only band-to-band recombination. From narrowest to widest the curves are for currents of 20, 40, and 60 mA.

We assume that Nakamura did not observe the overlap of the relative intensity plots at higher currents because either the doping of the active region was not low enough to cause strong saturation at the currents applied, or there were many other recombination mechanisms in the energy gap which we did not consider. The tails at lower energy that Nakamura observed in his intensity spectra are not present in our results because we considered the impurity level as a delta function when in reality this level is broadened.[33] Band tails at the energy band edges are not the cause of the broadening because the dopants are very effectively screened by the large charge carrier concentration in the active region.

There are many energy states in the band gap for radiative and nonradiative recombination which we did not include. GaN has states in the energy gap due to nitrogen vacancies, nitrogen substitutional on metal sites, metal substitutional on nitrogen sites, and metal vacancies.[36,27] The materials we have simulated are actually alloys of GaN with AlN or InN. However, we assume that since the fraction of GaN is much larger than the other compounds, the alloy will exhibit mostly GaN properties. The metal substitutional on nitrogen sites also introduces tails in absorption plots[36] and may be the reason that the experimental results of Nakamura has long-wavelength tails in the emission spectra which we do not observe in our simulations.

The power calculated here is somewhat higher than the experimental results of Nakamura. For instance at 10 mA we obtained an output power of 14.2 mW, while Nakamura[1] obtained an output power of 0.85 μW. Also, at 40 mA, we obtained an output power of 51.8 mW while Nakamura obtained an output power of 2.5 mW. This difference may be due to several reasons. We do not have the actual doping values and complete dimensions of his device. Metal contacts to nitride based semiconductors form Schottky contacts and have large contact resistances. Furthermore, other recombination mechanisms, broadening of the acceptor level, and current transport mechanisms such as electron transport at autodoping centers[39] should be included. Finally, better values for the parameters used in the model are needed.

VI. CONCLUSION

We have performed a complete one dimensional numerical simulation of a wide band-gap light-emitting diode structure which includes stopper layers around the active region for greater carrier confinement. Tunneling of charge carriers and recombination at impurity levels were also included. A new highly convergent, fast, and memory efficient algorithm is described and used for the simulation. The results demonstrate that greater power is emitted in band-to-band recombination processes than band-to-impurity recombination, and that the output power versus current curves begin to saturate at high currents in the band-to-impurity recombination case. This saturation is due to charge carriers leaking out of the active region by surmounting the stopper layers and is controlled by changing the active region thickness and impurity concentrations. Also, the optical emission spectra is modified by changing the active region thickness and impurity concentrations. These results demonstrate the importance of full numerical simulation in predicting power saturation characteristics and the shape of the emission spectra.

ACKNOWLEDGMENTS

This work was supported by a grant from the Army Research Office. K. Hess, G. H. Song, and M. Grupen were supported by the NSF-ERC at the University of Illinois.

[1] S. Nakamura, T. Mukai, and M. Senoh, Appl. Phys. Lett. **64**, 1687 (1994).
[2] M. Asif Khan, A. Bhattarai, J. N. Kuznia, and D. T. Olson, Appl. Phys. Lett. **63**, 1214 (1993).
[3] M. Asif Khan, J. N. Kuznia, D. T. Olson, J. M. Van Hove, M. Blasingame, and L. F. Reitz, Appl. Phys. Lett. **60**, 2917 (1992).
[4] H. Amano, T. Tanaka, Y. Kunii, K. Kato, S. T. Kim, and I. Akasaki, Appl. Phys. Lett. **64**, 1377 (1994).
[5] G. H. Song, Ph.D. thesis, University of Illinois, Urbana-Champaign, Illinois, 1990.
[6] S. Nakamura, J. Cryst. Growth **145**, 911 (1994).
[7] S. Nakamura, T. Mukai, and M. Senoh, Jpn. J. Appl. Phys. **30**, L1998 (1991).
[8] I. Akasaki, H. Amano, H. Murakami, M. Sassa, H. Kato, and K. Manabe, J. Cryst. Growth **128**, 379 (1993).
[9] N. Koide, H. Kato, M. Sassa, S. Yamasaki, K. Manabe, M. Hashimoto, H. Amano, K. Hiramatsu, and I. Alasaki, J. Cryst. Growth **115**, 639 (1991).
[10] S. Nakamura, M. Senoh, and T. Mukai, Jpn. J. Appl. Phys. **32**, L8 (1993).
[11] Y. Koide, H. Itoh, M. R. H. Khan, K. Hiramatu, N. Sawaki, and I. Akasaki, J. Appl. Phys. **61**, 4540 (1987).
[12] E. A. Albanesi, W. R. L. Lambrecht, and B. Segall, Phys. Rev. B **48**, 17841 (1993).
[13] G. Martin, S. Strite, A. Botchkarev, A. Agrawal, A. Rockett, W. R. L. Lambrecht, B. Segall, and H. Morkoc, J. Electron. Mater. **24**, 225 (1995).
[14] J. Baur, M. Kunzer, K. Maier, U. Kaufmann, and J. Schneider, Mater. Sci. Eng. **B29**, 61 (1995).
[15] W. A. Harrison, J. Vac. Sci. Technol. **14**, 1016 (1977).
[16] Matt Grupen, Ph.D. thesis, University of Illinois, Urbana, Illinois, 1994.
[17] G. P. Agrawal and N. K. Dutta, *Semiconductor Lasers* (Van Nostrand Rhinhold, New York, 1993).
[18] H. C. Casey, Jr. and M. B. Panish, *Heterostructure Lasers, Part A* (Academic, New York, 1978).
[19] M. Asif Khan, Q. Chen, R. A. Skogman, and J. N. Kuznia, Appl. Phys. Lett. **66**, 2046 (1995).
[20] A. S. Barker and M. Ilegems, Phys. Rev. B **7**, 743 (1973).
[21] V. W. L. Chin, T. L. Tansley, and T. Osotchan, J. Appl. Phys. **75**, 7365 (1994).
[22] R. F. Davis, Phys. B **185**, 1 (1993).
[23] T. Detchprohm, K. Hiramatsu, N. Sawaki, and I. Akasaki, J. Cryst. Growth **145**, 192 (1994).
[24] R. Dingle and M. Ilegems, Solid State Commun. **9**, 175 (1971).
[25] J. Edwards, K. Kawabe, G. Stevens, and R. H. Tredgold, Solid State Commun. **3**, 99 (1965).
[26] C. P. Foley and T. L. Tansley, Phys. Rev. B **33**, 1430 (1986).
[27] P. Hacke, T. Detchprohm, K. Hiramatsu, N. Sawaki, K. Tadatomo, and K. Miyake, J. Appl. Phys. **76**, 304 (1994).
[28] W. A. Harrison, *Electronic Structure and the Properties of Solids: The Physics of the Chemical Bond* (Freeman, San Francisco, 1980).
[29] S. Logothetidis, J. Petalas, M. Cardona, and T. D. Moustakas, Phys. Rev. B **50**, 18017 (1994).
[30] H. Morkoc, S. Strite, G. B. Gao, M. E. Lin, B. Sverdlov, and M. Burns, J. Appl. Phys. **76**, 1363 (1994).
[31] S. Nakamura, Y. Harada, and M. Senoh, Appl. Phys. Lett. **58**, 2021 (1991).
[32] J. W. Orton, Semicond. Sci. Technol. **10**, 101 (1995).
[33] D. L. Orth, R. J. Mashl, and J. L.Skinner, J. Phys.-Condensed Matter **5**, 2533 (1993).
[34] J. I. Pankove, S. Bloom, and G. Harbeke, RCA Rev. **36**, 163 (1975).
[35] C. M. Wolfe, N. Holonyak, Jr., and G. E. Stillman *Physical Properties of Semiconductors* (Prentice–Hall, Englewood Cliffs, NJ, 1989).
[36] T. L. Tansley and R. J. Egan, Physica B **185**, 190 (1993).
[37] T. L. Tansley and C. P. Foley, J. Appl. Phys. **59**, 3241 (1986).
[38] H. Yamashita, K. Fukui, S. Misawa, and S. Yoshida, J. Appl. Phys. **50**, 896 (1979).
[39] R. J. Molnar, T. Lei, and T. D. Moustakas, Appl. Phys. Lett. **62**, 72 (1993).